J|A|C|S
ARTICLES
Published on Web 08/08/2002

^{13}C and ^{15}N Chemical Shift Tensors in Adenosine, Guanosine Dihydrate, 2′-Deoxythymidine, and Cytidine

Dirk Stueber and David M. Grant*

Contribution from the Department of Chemistry, University of Utah, 315 South 1400 East, Salt Lake City, Utah 84112-0850

Received November 6, 2001. Revised Manuscript Received June 10, 2002

Abstract: The ^{13}C and ^{15}N chemical shift tensor principal values for adenosine, guanosine dihydrate, 2′-deoxythymidine, and cytidine are measured on natural abundance samples. Additionally, the ^{13}C and ^{15}N chemical shielding tensor principal values in these four nucleosides are calculated utilizing various theoretical approaches. Embedded ion method (EIM) calculations improve significantly the precision with which the experimental principal values are reproduced over calculations on the corresponding isolated molecules with proton-optimized geometries. The ^{13}C and ^{15}N chemical shift tensor orientations are reliably assigned in the molecular frames of the nucleosides based upon chemical shielding tensor calculations employing the EIM. The differences between principal values obtained in EIM calculations and in calculations on isolated molecules with proton positions optimized inside a point charge array are used to estimate the contributions to chemical shielding arising from intermolecular interactions. Moreover, the ^{13}C and ^{15}N chemical shift tensor orientations and principal values correlate with the molecular structure and the crystallographic environment for the nucleosides and agree with data obtained previously for related compounds. The effects of variations in certain EIM parameters on the accuracy of the shielding tensor calculations are investigated.

Introduction

^{13}C and ^{15}N chemical shift tensor principal values and the orientations of the principal tensor components within a certain molecular framework are remarkably sensitive to electronic structure and intermolecular interactions.[1,2] This sensitivity makes the measurement of chemical shift tensors in solid-state NMR experiments an invaluable tool in the elucidation of molecular structure in biologically relevant molecules. Especially the large chemical shift anisotropy of the ^{15}N nucleus and its strong sensitivity to interactions involving the lone pair on the nitrogen atom are responsible for the fact that ^{15}N chemical shift tensors represent an excellent probe for electronic structure and intermolecular interactions.[3−6] Experimental ^{13}C and ^{15}N chemical shift tensor data are effectively complemented by quantum mechanical chemical shielding tensor calculations.[2,7,8] Solid-state NMR experiments can determine chemical shift tensor orientations only in relatively large single crystals.[9−11] However, for the vast majority of solids suitable crystals are unavailable and the NMR experiments are performed on powdered solids. For these samples, the calculations can be utilized to assign the chemical shift tensor orientations in the molecular framework.[3,12−14] Furthermore, the calculations can provide valuable information on the relationships between the experimental chemical shifts and molecular geometry and environment. However, finding good agreement between the experimental and calculated principal values is essential for a reliable assignment of the chemical shift tensor orientations and for a proper interpretation of the chemical shift tensor data in terms of molecular structure. Preliminary results on ionic[15−17] and on neutral polar[4−6,13,18−20] systems clearly show that the inclusion of intermolecular

* To whom correspondence should be addressed. Fax: (801)581-8433. E-mail: grant@chem.utah.edu.

(1) Grant, D. M. In *Encyclopedia of NMR*; Grant, D. M., Harris, R. K., Eds.; John Wiley: Chichester, 1996; Vol. 2, pp 1298−1312.
(2) de Dios, A. C.; Oldfield, E. *Solid State Nucl. Magn. Reson.* **1996**, *6*, 101−125.
(3) Solum, M.; Altman, K. L.; Strohmeier, M.; Berges, D. A.; Zhang, Y. Z.; Facelli, J. C.; Pugmire, R. J.; Grant, D. M. *J. Am. Chem. Soc.* **1997**, *119*, 9804−9809.
(4) Anderson-Altman, K.; Phung, C. G.; Mavromoustakes, S.; Zheng, Z.; Facelli, J. C.; Poulter, C. D.; Grant, D. M. *J. Am. Chem. Soc.* **1995**, *99*, 10454−10458.
(5) Facelli, J. C.; Pugmire, R. J.; Grant, D. M. *J. Am. Chem. Soc.* **1996**, *118*, 5488−5489.
(6) Hu, J. Z.; Facelli, J. C.; Alderman, D. W.; Pugmire, R. J.; Grant, D. M. *J. Am. Chem. Soc.* **1998**, *120*, 9863−9869.
(7) Facelli, J. C. *J. Biomol. Struct. Dyn.* **1998**, *16*, 619−629.
(8) Facelli, J. C.; Hu, J. H.; Solum, M. S.; Pugmire, R. J.; Grant, D. M. In *Modeling NMR Chemical Shifts*; Facelli, J. C., de Dios, A. C., Eds.; ACS Symposium Series Vol. 732; American Chemical Society: Washington, DC, 1999; pp 162−176.
(9) Carter, C. M.; Facelli, J. C.; Alderman, D. W.; Dalley, N. K.; Wilson, B. E.; Grant, D. M. *J. Chem. Soc, Faraday Trans. 1* **1988**, *84*, 3673−3690.
(10) Liu, F.; Phung, C. G.; Alderman, D. W.; Grant, D. M. *J. Am. Chem. Soc.* **1996**, *118*, 10629−10634.
(11) Liu, F.; Phung, C. G.; Alderman, D. W.; Grant, D. M. *J. Magn. Reson., Ser. A* **1996**, *120*, 231−241.
(12) Veeman, W. S. *Carbon-13 Chemical Shift Anisotropy*; Academic Press: San Francisco, 1984; Vol. 16.
(13) Gu, Z.; McDermott, A. E.; Facelli, J. C. *Mol. Phys.* **1995**, *86*, 865−872.
(14) Wei, Y.; de Dios, A. C.; McDermott, A. E. *J. Am. Chem. Soc.* **1999**, *121*, 10389−10394.
(15) Stueber, D.; Orendt, A. M.; Facelli, J. C.; Parry, R. W.; Grant, D. M. *Solid State Nucl. Magn. Reson.* **2001**.
(16) Orendt, A. M.; Facelli, J. C.; Grant, D. M. *Chem. Phys. Lett.* **1999**, *302*, 499−504.
(17) Nicholas, J. B.; Xu, T.; Barich, D. H.; Torres, P. D.; Haw, J. F. *J. Am. Chem. Soc.* **1996**, *118*, 4202−4203.
(18) Stueber, D.; Grant, D. M. *Solid State Nucl. Magn. Reson.* **2001**.
(19) de Dios, A. C.; Pearson, J. G.; Oldfield, E. *Science* **1993**, *260*, 1491−1496.

interactions in chemical shift tensor calculations is essential for reproducing accurately experimental principal values. The embedded ion method (EIM), as a general method to include efficiently intermolecular interactions in quantum mechanical chemical shift tensor calculations on ionic and molecular polar systems, was recently developed in our laboratory.[21] The EIM simulates the electrostatic crystal potential that is experienced by each atom in a molecule or ion of interest inside an infinite crystal lattice with a finite, self-consistent array of point charges, which is generated using the Ewald summation method.[22] Subsequently, the chemical shift tensors are calculated for the ion or molecule of interest embedded inside the point charge array using standard quantum mechanical methods. The EIM was developed and first tested for a series of ionic potassium carbonates and thiocarbonates and significantly improved the accuracy of ^{13}C chemical shift tensor calculations for these ionic compounds.[15] Furthermore, the EIM has been applied on several neutral derivatives of the ionic carbonates and thiocarbonates with comparable success, revealing that chemical shifts are sensitive to electrostatic crystal potentials even for neutral species with relatively weak intermolecular interactions.[18] The results obtained in the present study demonstrate the applicability of the EIM on relatively large molecular systems, such as the nucleosides that involve strong intermolecular hydrogen bonding.

The study of nucleosides and nucleotides as building blocks of DNA has been of considerable interest[23−26] since their role in the structure of DNA first was proposed by Watson and Crick in 1953.[27] However, only very little ^{13}C and ^{15}N experimental and theoretical chemical shift tensor data are available for nucleosides, nucleotides, and related compounds.[3−7] This discrepancy can mainly be attributed to the relatively large size of these molecules, the low NMR sensitivity of especially the ^{15}N nucleus, and the disadvantageous long T_1 relaxation times that are very often exhibited in these compounds. The present study reports the measurement of the ^{13}C and ^{15}N chemical shift tensor principal values for adenosine (A), guanosine dihydrate (Gdh), 2′-deoxythymidine (dT), and cytidine (C). Figure 1 shows the Lewis structures and atom numbering schemes for these four nucleosides. The ^{13}C and ^{15}N principal values are measured by utilizing the 2-D FIREMAT[28] and 1-D slow-spinning experiments, respectively, for natural abundance samples. Furthermore, the ^{13}C and ^{15}N chemical shielding tensor principal values are calculated employing several different theoretical approaches. The accuracy with which the experimental shift principal values are reproduced in EIM calculations is investigated, and the contribution to chemical shielding that can be attributed to intermolecular interactions is estimated. The sensitivity of EIM calculations to the size and self-consistency of the point charge arrays that are utilized in these calculations is also explored.

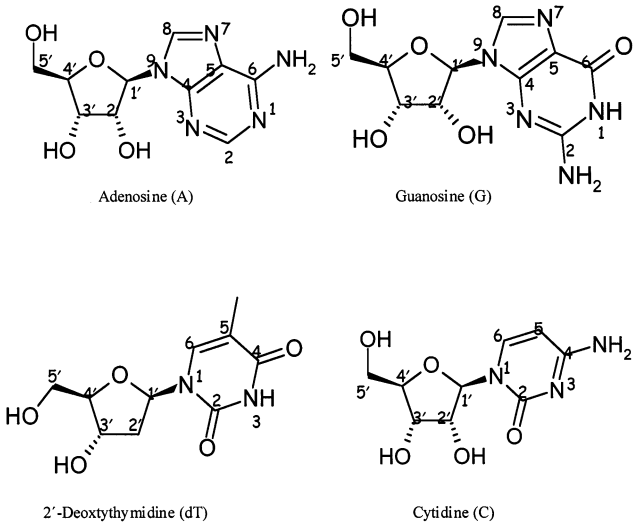

Figure 1. Structures and atom numbering schemes for adenosine, guanosine, 2′-deoxythymidine, and cytidine.

Furthermore, the various calculations are used to assign the ^{13}C and ^{15}N chemical shift tensor orientations in the molecular frames of the nucleic acid bases. These orientations and the magnitudes of the actual chemical shift principal values are correlated with electronic structure and intermolecular hydrogen bonding for the nucleosides under investigation.

Experimental Section

Materials. Samples of A, G, dT, and C were purchased from Aldrich. The commercial powdered samples of A, C, and dT were shown to be the desired anhydrous materials and were used in the NMR experiments without further purification. Relative humidity induces reversible crystal transitions of G among an anhydrous, an intermediate hydrated, and a dihydrated state.[29] Gdh was prepared by keeping the commercial sample in a desiccator for two months, immersed in a saturated water vapor atmosphere.

NMR Experiments. All NMR spectra were recorded on a Chemagnetics CMX-400 spectrometer at ^{13}C and ^{15}N frequencies of 100.62 and 40.55 MHz, respectively, using a Chemagnetics 7.5 mm PENCIL ROTOR probe. All experiments were performed utilizing standard cross polarization (CP) techniques and high-power TPPM[30,31] proton decoupling on natural abundance samples. High-speed CP magic-angle spinning (MAS) spectra utilizing the total suppression of sidebands (TOSS)[32] method were recorded of all samples to obtain the isotropic ^{13}C and ^{15}N chemical shift values and to ensure the identity and purity of the materials. The ^{13}C and ^{15}N chemical shift tensor principal values of the four nucleosides were extracted from 2-D FIREMAT experiments and measured in 1-D slow-spinning experiments, respectively. To ensure optimal experimental conditions, which was especially important for the ^{15}N natural abundance spectra, pulse delay times, contact times, decoupler frequencies, and the Hartman−Hahn matching conditions were optimized for each sample.

The T_1 proton relaxation times for A and C were estimated in two saturation recovery experiments to be longer than 200 and 160 s, respectively. Attempts to accurately measure the T_1 relaxation times for these two nucleosides were not undertaken. Instead, useful pulse delay times were determined in a series of high-speed ^{13}C CPMAS

(20) de Dios, A. C.; Laws, D. D.; Oldfield, E. *J. Am. Chem. Soc.* **1994**, *116*, 7784−7786.
(21) Stueber, D.; Guenneau, F. N.; Grant, D. M. *J. Chem. Phys.* **2001**, *114*, 9236−9243.
(22) Ewald, P. P. *Ann. Phys.* **1921**, *64*, 253−287.
(23) Dickerson, R. E.; Grzeskowiak, K.; Grzeskowiak, M.; Kopka, M. L.; Larsen, T.; Lipanov, A.; Privé, G. C.; Quintana, J.; Schultze, P.; Yanagi, K.; H., Y.; Yoon, H. C. *Nucleosides Nucleotides* **1991**, *10*, 3−24.
(24) Dickerson, R. E.; Drew, H. R.; Conner, B. N.; Wing, R. M.; Fratani, A. V.; Kopka, M. L. *Science* **1982**, *216*, 475−485.
(25) Dickerson, R. E. *Sci. Am.* **1983**, *249*, 94−111.
(26) Weinberg, R. A. *Sci. Am.* **1985**, *253*, 48−57.
(27) Watson, J. D.; Crick, F. *Nature* **1953**, *171*, 737−738.
(28) Alderman, D. W.; McGeorge, G.; Hu, J. Z.; Pugmire, R. J.; Grant, D. M. *Mol. Phys.* **1998**, *95*, 1113−1126.
(29) Sugawara, Y.; Yasuhiro, I.; Hitoshi, I.; Hisako, U.; Saito, H. *J. Biomol. Struct. Dyn.* **1994**, *11*, 721−729.
(30) Bennet, A. E.; Rienstra, C. M.; Auger, M.; Lakshmi, K. V.; Griffin, R. G. *J. Chem. Phys.* **1995**, *103*, 6951−6958.
(31) McGeorge, G.; Alderman, D. W.; Grant, D. M. *J. Magn. Reson.* **1999**, *137*, 138−143.
(32) Dixon, W. T. *J. Chem. Phys.* **1982**, *77*, 1800−1809.

Table 1. Acquisition Parameters Used in the ^{13}C 2-D FIREMAT Experiments[a]

nucleoside	sw_{acq}	sw_{ev}	pw (^1H)	pw (^{13}C)	ct	pd	al_{acq}	al_{ev}	ss
A	67.2	11.2	4.4	5.0	2.0	240	2048	16	700
Gdh	72.0	12.0	4.3	5.0	4.0	5	3072	16	750
dT	61.854	10.304	4.1	4.5	4.0	60	4096	32	322
C	47.386	7.898	4.1	4.4	4.0	180	4098	32	298

[a] Spectral widths (sw) are given in kHz, 90° pulse widths (pw) in μs, contact times (ct) in ms, pulse delay times (pd) in s, acquisition lengths (al) in number of collected points, and spinning speeds (ss) in Hz; acq and ev denote the acquisition and evolution dimensions, respectively.

Table 2. Acquisition Parameters Used in the ^{15}N 1-D Slow Spinning Experiments[a]

nucleoside	sw	pw (^1H)	ct	pd	al	ss
A	25.0	4.7	4.0	300	1500	730
Gdh	25.0	4.6	2.0	5	1500	1005
dT	12.165	4.2	4.0	60	1024	250
C	30.03	4.2	4.0	180	3072	298

[a] Spectral widths (sw) are given in kHz, 90° pulse widths (pw) in μs, contact times (ct) in ms, pulse delay times (pd) in s, acquisition lengths (al) in number of collected points, and spinning speeds (ss) in Hz.

experiments on each sample. In these experiments, the pulse delay times and the number of scans were incremented in such a way that the total time for each experiment in the series was constant. The pulse delays which resulted in the highest signal-to-noise ratios were chosen as pulse delays and were found to be 300 and 180 s for A and C, respectively. The T_1 proton relaxation times for Gdh and dT were measured in saturation recovery experiments and determined to be approximately 3 and 45 s, respectively. Accordingly, pulse delay times of 5 and 60 s, respectively, were used in all NMR experiments for these two nucleosides.

The acquisition parameters used in the ^{13}C 2-D FIREMAT experiments and in the ^{15}N 1-D slow-spinning experiments are summarized in Tables 1 and 2, respectively. The experimental ^{13}C and ^{15}N chemical shifts were externally referenced to the TMS scale using the CPMAS spectra of adamantane and glycine, respectively. The carbon peak at higher chemical shift in adamantane and the nitrogen peak in glycine are assumed to have a chemical shift of 38.56 ppm and −346.40 ppm with respect to TMS and NO_2CH_3, respectively. The chemical shift tensor principal values were extracted from the spinning sideband patterns recorded in the ^{15}N slow-spinning experiments utilizing the BANDED MATRIX[33] approach. The complex FIDs were simulated in least-squares fits obtained using a SIMPLEX algorithm. The ^{13}C chemical shift tensor principal values were extracted from the 2-D FIREMAT data sets as described previously.[28,34]

Theoretical Approaches

The various theoretical approaches utilized to calculate the ^{13}C and ^{15}N chemical shielding tensors for A, Gdh, dT, and C in this study, along with the corresponding abbreviations used in the remainder of this paper, are listed in Table 3. The shielding tensors were calculated for all four isolated nucleoside molecules with X-ray (ISO/X-RAY) and proton-optimized (ISO/H-OPT) geometries. In the latter case, the optimizations were also performed on isolated molecules. Another approach was to calculate the shielding tensors for the isolated nucleoside molecules utilizing proton-optimized geometries for A, Gdh, dT, and C obtained when the protons are optimized iteratively inside a point charge array until self-consistency is reached (ISO/H-OPT/4). Intermolecular interactions in the shielding tensor calculations were simulated with electrostatic crystal potentials by utilizing the EIM (EIM/H-OPT/4). The accuracies with which these four approaches reproduce the experimental principal values are determined in shielding-shift correlations and compared based upon the corresponding slopes, intercepts, and root-mean-square (rms) values obtained in linear fits. The comparison is employed to estimate the effects of intermolecular hydrogen bonding on chemical shielding in the nucleosides and to determine if the EIM is capable of simulating these effects. Also, the sensitivity of chemical shielding tensor calculations to accurate proton positions is explored. To investigate the correlation between the point charge array size and the accuracy with which the experimental principal values are calculated in the EIM, the Ewald parameter that defines the total number of point charges in the array, N, is varied in EIM calculations on A, dT, and C (EIM/H-OPT/2, EIM/H-OPT/3, EIM/H-OPT/4). Furthermore, since it is known that the most significant relative changes in the partial NBO atomic charges are observed in the first iteration of the EIM,[21,15] the necessity of conducting the iteration procedure in the EIM until self-consistency is reached is also explored for A, dT, and C. This was accomplished by performing chemical shielding tensor calculations in the first iteration of the EIM (EIM-1/H-OPT/3 and EIM-1/H-OPT/4) and comparing the principal values obtained with those obtained in EIM calculations utilizing self-consistent point charge arrays (EIM/H-OPT/3 and EIM/H-OPT/4). The neutron diffraction geometry for A[35] provides accurate proton positions. These proton positions are used to investigate if the EIM/H-OPT/4 calculations reproduce the neutron positions more accurately than the ISO/H-OPT calculations, as anticipated. Moreover, the availability of accurate proton positions allows for an accurate determination of the effects of intermolecular hydrogen bonding on chemical shielding, since shortcomings in the calculations arising from inaccurate proton positions are eliminated.

Calculations

Embedded Ion Method. The EIM[21] uses a modified version of the Ewald program[36,37] in conjunction with the quantum mechanics program Gaussian 98.[38] Ewald is utilized to generate finite point charge arrays with partial NBO[39−46] atomic charges at the crystallographic atom positions. These point charge arrays simulate the electrostatic Ewald potential that is experienced by a molecule of interest inside an infinite crystal lattice. Gaussian 98 is employed to quantum mechanically calculate the partial NBO atomic charges and the chemical shift tensors for the molecule of interest embedded inside the point charge array.

The computational process to calculate chemical shielding tensors in the EIM involves three steps.[21] In the initial step, the proton positions of the X-ray geometry are optimized and partial NBO atomic charges are calculated for the isolated nucleoside molecule under investigation

(33) Sethi, N. K.; Alderman, D. W.; Grant, D. M. *Mol. Phys.* **1990**, *71*, 217−238.
(34) Alderman, D. W.; Solum, M. S.; Grant, D. M. *J. Chem. Phys.* **1986**, *84*, 3717−3725.
(35) Klooster, W. T.; Ruble, J. R.; Craven, B. M. *Acta Crystallogr., Sect. B* **1991**, *47*, 376−383.
(36) Derenzo, S. E.; Klintenberg, M. K.; Weber, M. J. *J. Chem. Phys.* **2000**, *112*, 2074−2081.
(37) Klintenberg, M.; Derenzo, S. E.; Weber, M. J. *J. Comput. Phys. Commun.* **2000**, *131*, 120−128.
(38) Frisch, M. J.; Trucks, G. W.; Schlegel, H. B.; Scuseria, G. E.; Robb, M. A.; Cheeseman, J. R.; Zakrzewski, V. G.; Montgomery, J. A., Jr.; Stratmann, R. E.; Burant, J. C.; Dapprich, S.; Millam, J. M.; Daniels, A. D.; Kudin, K. N.; Strain, M. C.; Farkas, O.; Tomasi, J.; Barone, V.; Cossi, M.; Cammi, R.; Mennucci, B.; Pomelli, C.; Adamo, C.; Clifford, S.; Ochterski, J.; Petersson, G. A.; Ayala, P. Y.; Cui, Q.; Morokuma, K.; Malick, D. K.; Rabuck, A. D.; Raghavachari, K.; Foresman, J. B.; Cioslowski, J.; Ortiz, J. V.; Baboul, A. G.; Stefanov, B. B.; Liu, G.; Liashenko, A.; Piskorz, P.; Komaromi, I.; Gomperts, A.; Martin, R. L.; Fox, D. J.; Keith, T.; Al-Laham, M. A.; Peng, C. Y.; Nanayakkara, A.; Gonzalez, C.; Challacombe, M.; Gill, P. M. W.; Johnson, B.; Chen, W.; Wong, M. W.; Andres, J. L.; Gonzales, C.; Head-Gordon, M.; Replogle, E. S.; Pople, J. A. *Gaussian 98*, revision A.7; Gaussian, Inc.: Pittsburgh, PA, 1998.
(39) Carpenter, J. E.; Weinhold, F. J. *THEOCHEM* **1988**, *169*, 41−62.
(40) Carpenter, J. E. University of Wisconsin, Madison, WI, 1987.
(41) Foster, J. P.; Weinhold, F. *J. Am. Chem. Soc.* **1980**, *102*, 7211−7218.
(42) Reed, A. E.; Weinhold, F. *J. Chem. Phys.* **1983**, *78*, 4066−4073.
(43) Reed, A. E.; Weinhold, F. *J. Chem. Phys.* **1985**, *83*, 1736−1740.
(44) Reed, A. E.; Weinstock, R. B.; Weinhold, F. *J. Chem. Phys.* **1985**, *83*, 735−746.
(45) Reed, A. E.; Curtiss, L. A.; Weinhold, F. *Chem. Rev.* **1988**, *88*, 899−926.
(46) Weinhold, F.; Carpenter, J. E. In *Plenum 227*; 1988.

Table 3. Various Theoretical Approaches Utilized to Calculate the ^{13}C and ^{15}N Chemical Shielding Tensors for A, Gdh, dT, and C in This Study, along with the Corresponding Abbreviations[a]

abbreviation	nucleosides	method	geometry	N_i	N
ISO/X-RAY	A, Gdh, dT, C	isolated molecule	X-ray diffraction		
ISO/H-OPT	A, Gdh, dT, C	isolated molecule	proton-optimized		
ISO/H-OPT/4	A, Gdh, dT, C	isolated molecule	self-consistent proton positions	>1[b]	4
EIM-1/H-OPT/ 3	A, dT, C	EIM	iteration-1 proton positions	1	3
EIM/H-OPT/3	A, dT, C	EIM	self-consistent proton positions	>1[b]	3
EIM-1/H-OPT/ 4	A, dT, C	EIM	iteration-1 proton positions	1	4
EIM/H-OPT/4	A, Gdh, dT, C	EIM	self-consistent proton positions	>1[b]	4
ISO/NEU	A	isolated molecule	neutron diffraction		
EIM/NEU/4	A	EIM	neutron diffraction	>1[b]	4

[a] The numbers behind the second backslash in the abbreviations denote the value used for the Ewald parameter, *N*. [b] Self-consistent point charge arrays are generated. For actual N_i values, see Results and Discussion.

using Gaussian 98. In the second step, a series of iterations between Ewald and Gaussian 98 is conducted to produce an array that contains self-consistent point charges. The initial NBO charges and the atom positions of the hydrogen-optimized geometry are used as point charge values and crystallographic coordinates in Ewald, respectively, to generate an initial point charge array. The point charges inside this array that correspond to the atom positions of the nucleoside molecule of interest, positioned in the central region of the array, are replaced with the corresponding "real" atoms. Subsequently, a second calculation of NBO charges and a second optimization of the proton positions are performed using Gaussian 98 with the nucleoside molecule embedded inside the central region of the point charge array. This completes the first iteration. The atomic charges and proton positions obtained in the first iteration differ slightly from the corresponding initial values and are used as input values in the Ewald calculation of the second iteration. This iteration procedure between the two programs is repeated N_i times, until the atomic charges and proton positions calculated with Gaussian 98 are self-consistent. Self-consistency of partial atomic charges is assumed when the differences of partial charges between consecutive iterations are below 0.001 *e*. In the final step of the EIM, the point charges in the self-consistent array that correspond to the nucleoside molecule of interest are again replaced with real atoms, and the chemical shielding tensor calculation on this nucleoside molecule embedded inside the central region of the point charge array is performed in Gaussian 98. The EIM calculations on Gdh are performed on a fragment consisting of one G molecule and the corresponding stoichiometric two water molecules.

In the ISO/H-OPT/4 calculations on the nucleosides, the proton positions are optimized in the iteration procedure described above; hence, each iteration step included an optimization of the proton positions in addition to the calculation of partial atomic charges. The shielding tensors in the ISO/H-OPT/4 calculations are subsequently computed for the isolated nucleoside molecules.

Ewald Program. The Ewald program initially generates a finite array of point charges by replicating the crystallographic unit cell for the nucleoside crystal under investigation with partial NBO atomic charges at the crystallographic atom positions. $8N^3$ unit cells are reproduced in the positive and negative directions of the crystallographic axis system. The entire array is divided into three zones. Zone 1 is spherical in shape with the center of the sphere located at the origin of the array and contains N_1 point charges. Zone 2, containing N_2 point charges, is also a sphere, surrounding zone 1. The number of point charges in zones 1 and 2 together is $N_C = N_1 + N_2$, with $N_1 < N_2$. Zone 3 is the region between the outer boundary of zone 2 and the boundary of the entire array formed by the $8N^3$ unit cells. Accordingly, the total number of point charges in the array, N_T, is given by $N_T = 8N^3N_{uc}$, where N_{uc} denotes the number of point charges per unit cell. Subsequently, the Ewald program computes the Ewald potential at the crystallographic sites in zones 1 and 2, which corresponds to the infinite crystal lattice, using the Ewald summation method. Finally, the values of the point charges in zone 3 are varied as the actual fitting parameters of the program. They are calculated from $N_T - N_C$ linear, simultaneous, homogeneous equations to reproduce the Ewald potential at the crystallographic sites in zones 1 and 2 with an accuracy that depends on the sizes of zones 1, 2, and 3. [21,36] This accuracy is monitored by comparing the actual Ewald potential with the potential produced by the finite point charge array. The two potentials are calculated at 1000 randomly chosen checkpoints in zone 1 and an rms value for the deviation of the fitted potential from the Ewald potential at these 1000 points is computed.

Quantum Mechanical Calculations. The proton optimizations, gauge invariant atomic orbital (GIAO)[47] chemical shielding tensor calculations, and calculations of NBO partial atomic charges are performed at the B3LYP[48−51]/D95**[52] level of theory utilizing the Gaussian 98 package. The B3LYP/D95** level of theory was chosen based upon the results previously obtained in our laboratory[53,54] and elsewhere.[55,56] These data show that this level reproduces ^{13}C and ^{15}N chemical shift tensor principal values with good accuracy, at acceptable computational costs. The NBO method was selected to calculate the partial atomic charges since this method exhibits a relatively small basis set dependence, while requiring a reasonably low computational effort.[44,57−59] Because absolute atomic charge values are used in the Ewald summation method to calculate the Ewald potential, the EIM is sensitive to the theoretical method of calculating these partial atomic charges. This sensitivity has not yet been explored by the authors; however, it will be one of the key objectives in further evaluating the EIM in the future. To date, the applicability of the method using NBO charges on a wide variety of different compounds with remarkable success has been demonstrated.

Results and Discussion

Experimental NMR Results and Spectral Assignments. Figures 2 and 3 show for dT the ^{13}C high-speed TOSS CPMAS spectrum and the ^{13}C isotropic and anisotropic spectra that were extracted from the 2-D FIREMAT data set, respectively. ^{13}C TOSS CPMAS and FIREMAT spectra similar in quality were recorded for A, Gdh, and C. The CPMAS spectrum of dT

(47) Ditchfield, R. *Mol Phys.* **1974**, *27*, 789−807.
(48) Becke, A. D. *J. Chem. Phys.* **1993**, *98*, 5648−5652.
(49) Lee, C.; Yang, W.; Parr, R. G. *Phys. Rev. B* **1988**, *37*, 785−789.
(50) Becke, A. D. *Phys. Rev. A* **1988**, *38*, 3098−3100.
(51) Miehlich, B.; Savin, A.; Stoll, H.; Preuss, H. *Chem. Phys. Lett.* **1989**, *157*, 200−206.
(52) Dunning, T. H.; Hay, P. J. *Modern Theoretical Chemistry III*; Plenum Press: New York, 1976.
(53) Harper, K. J.; McGeorge, G.; Grant, D. M. *J. Am. Chem. Soc.* **1999**, *121*, 6488−6496.
(54) Harper, K. J.; McGeorge, G.; Grant, D. M. *Magn. Reson. Chem.* **1998**, *36*, 135−134.
(55) Cheeseman, J. R.; Trucks, G. W.; Keith, T.; Frisch, M. J. *J. Chem. Phys.* **1996**, *104*, 5497−5509.
(56) Dobalik, A.; Kalchhauser, H.; Mikenda, W.; Schwenk, G. *Magn. Reson. Chem.* **1999**, *37*, 895−902.
(57) Wiberg, K. B.; Rablen, P. R. *J. Comput. Chem.* **1993**, *14*, 1504−1518.
(58) van Alem, K.; Sudhoelter, E. J. R.; Zuilhof, H. *J. Phys. Chem. A* **1998**, *102*, 10860−10868.
(59) van Alem, K.; Lodder, G.; Zuilhof, H. *J. Phys. Chem. A* **2000**, *104*, 2780−2787.

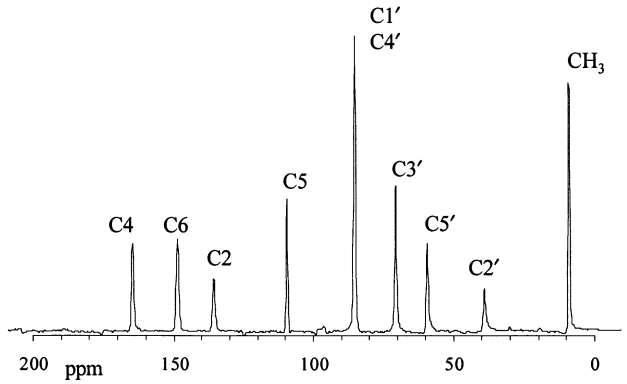

Figure 2. The ^{13}C TOSS CPMAS spectrum of dT along with the corresponding assignments of the isotropic resonances.

illustrates the distinct spectral separation of the isotropic chemical shifts for the sugar carbons and the carbon atoms of the nucleic acid bases. Furthermore, the spectrum reveals the homogeneous broadening of the base carbon signals due to directly bonded ^{14}N. The coupling of the ^{13}C nucleus to the quadrupolar ^{14}N isotope is neglected in the fitting procedures to extract the ^{13}C chemical shift tensor principal values. The resulting broader and slightly distorted lines are estimated to introduce an error of approximately 5 ppm into the principal values for the affected tensors. The sugar carbons in dT exhibit relatively narrow lines, except for C2′ and C5′. The wider peaks observed for these two CH_2 resonances can most likely be attributed to insufficient proton decoupling. The position and the width of the spectral window in the isotropic evolution dimension of the ^{13}C FIREMAT experiment on dT were chosen so that the "sugar region" of the spectrum is superimposed on the "base region" without overlapping peaks, as is shown in Figure 3. This allowed for the utilization of a relatively slow spinning speed[28] (see Table 2) and the description of the relatively narrow CH_3 tensor with a sufficient number of sidebands. The spinning sideband patterns for the sugar carbon atoms experience a relatively high signal-to-noise ratio. Larger chemical shift anisotropies and directly bonded ^{14}N nuclei reduce the intensity of the spinning sidebands for the base carbons accordingly. On the other hand, these extremely wide tensors are described by an appreciable number of sidebands, compensating for the loss in intensity.

The high-speed ^{13}C TOSS CPMAS spectrum recorded of the commercial G sample is shown in Figure 4a. The immensely broadened peaks and the fine structure indicate a nonstoichiometrical state of hydration. The appearance of the TOSS CPMAS spectrum of G changes considerably after the sample is stoichiometrically hydrated to the dihydrated form. The corresponding spectrum is shown in Figure 4b. The lines narrow substantially, and most of the fine structure of the peaks disappeared. However, four lines still exhibit some splitting, which can be attributed to the presence of two molecules per asymmetric unit in the crystal lattice of Gdh.[60] The spectrum of Gdh acquired in this study agrees with a spectrum of Gdh recorded by Sugawara et al.[29] Furthermore, the assignments of the ^{13}C resonances to atomic positions according to the results obtained in the EIM calculations in the present study are in agreement with the assignments reported by Sugawara et al.[29]

Figure 5 shows the ^{15}N 1-D slow-spinning spectrum for dT. The spinning sideband patterns for the 2 nitrogens in dT are well separated and sufficient in signal-to-noise to allow for the extraction of the principal values with an estimated accuracy of ± 3 ppm. Similar ^{15}N slow-spinning spectra were recorded of C and A. Due to the increasing number of nitrogens in these two nucleosides, the suitable spinning speeds that separate sufficiently the corresponding sidebands become higher. However, even in the spectrum for A with 5 nitrogens, the sidebands can be sufficiently separated using a spinning speed of 730 Hz. The presence of two molecules per asymmetric unit in the crystal lattice of Gdh doubles the number of potential ^{15}N resonances to 10, and in fact, all 10 resonances are resolved in the 1-D slow-spinning experiment. Due to the large number of lines in the 1-D spectrum, a relatively high spinning speed of 1005 Hz had to be utilized to achieve sufficient separation. This spinning speed reduces the number of sidebands for the narrow NH_2 tensors, and the certainty of the corresponding principal values is decreased to approximately ± 5 ppm. Figure 6 shows the ^{15}N slow-spinning spectrum of Gdh. The sideband patterns for the 10 magnetically nonequivalent nitrogen atoms are superimposed on each other with the individual sidebands sufficiently resolved to extract the corresponding principal values based upon the theoretical results obtained in the shielding tensor calculations.

The experimental ^{13}C and ^{15}N chemical shift tensor principal values, the corresponding averages, and the isotropic MAS chemical shift values obtained in this study are given in Tables 4−7 for A, Gdh, dT, and C, respectively. In the tables, δ_{11}, δ_{22}, and δ_{33} denote the chemical shift tensor principal values highest, intermediate, and lowest in shift, respectively, that is, $\delta_{11} \geq \delta_{22} \geq \delta_{33}$. For comparison purposes, Tables 4−7 also show the previously measured isotropic solution ^{13}C and ^{15}N chemical shift values.[61,62] The assignments of the ^{13}C and ^{15}N isotropic CPMAS chemical shifts and the principal values to atomic positions are based upon the results obtained in the EIM/H-OPT/4 calculations.

The principal values for three of the ^{13}C and for three of the ^{15}N shift tensors in the two distinct Gdh molecules per asymmetric unit[60] differ sufficiently to statistically assign these six tensors to each of the two Gdh molecules. A modified version of a program previously reported was utilized to complete these assignments.[11] The remaining tensors for equivalent atoms in the two distinct G molecules are indistinguishable.

For carbon atoms C6 and C2 in A, the isotropic chemical shifts differ only by 0.7 ppm and are barely resolved in the high-speed CPMAS spectrum. However, the corresponding two chemical shift tensors differ by 17, 33, and 14 ppm in the δ_{11}, δ_{22}, and δ_{33} principal values, respectively. These differences are sufficiently large to allow for clear assignments of the isotropic chemical shifts and the principal values to the two carbon atoms based upon the EIM/H-OPT/4 calculations.

The carbon atoms C1′ and C4′ in dT are separated by 3.4 ppm in solution, with C4′ at a higher chemical shift, whereas in the solid state, both carbons exhibit identical isotropic shifts. Nevertheless, the tensor principal values for C1′ and C4′ can be assigned utilizing the FIREMAT approach despite the fact

(60) Thewalt, U.; E., B. C.; Marsh, A. E. *Acta Crystallogr., Sect. B* **1970**, *26*, 1089−1101.
(61) Witanowski, M.; Stefaniak, L.; Webb, G. A. *Nitrogen NMR Spectroscopy*; Academic Press: San Diego, 1992; Vol. 25.
(62) Jones, A. J.; Grant, D. M.; Winkley, M. W.; Robins, R. K. *J. Phys. Chem.* **1970**, *92*, 4079−4087.

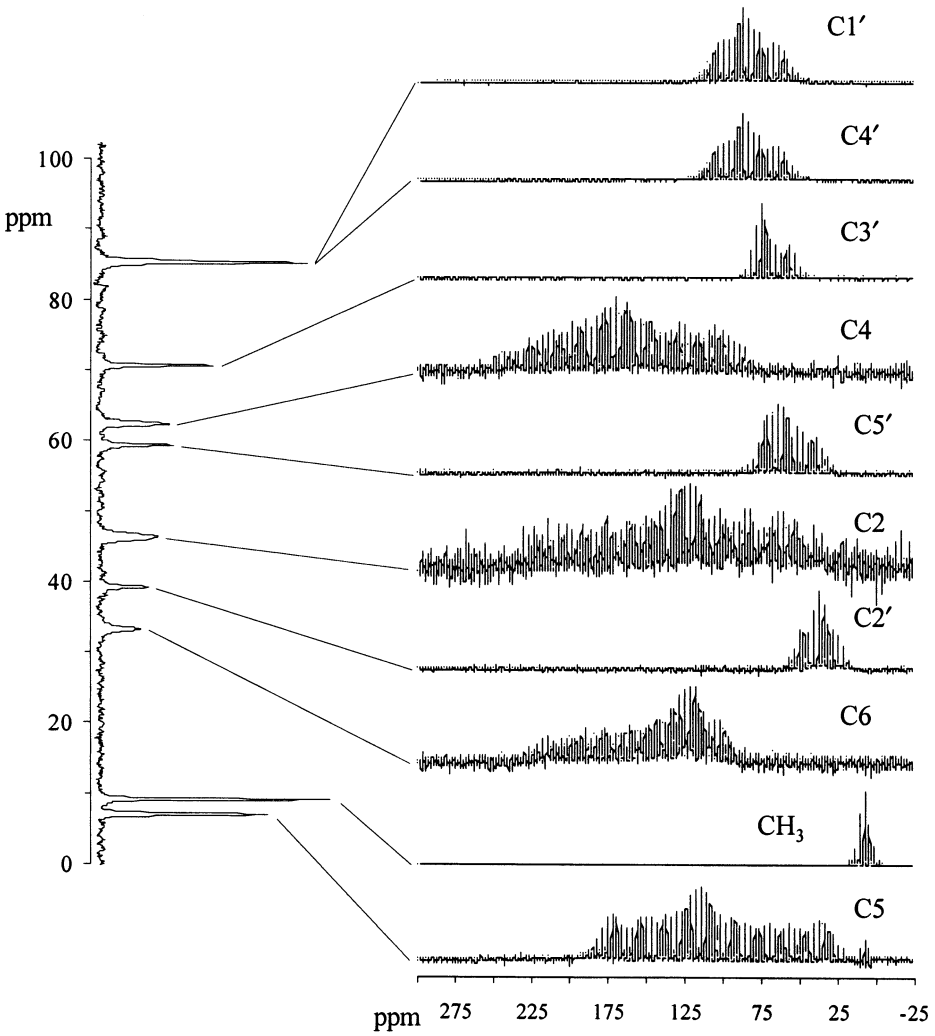

Figure 3. The ^{13}C isotropic and anisotropic spectra of dT extracted from the 2-D FIREMAT data set. Shown on the left is the isotropic "guide" spectrum (vertical), and on the right are the corresponding sideband patterns for each of the carbon atoms in the molecule. The assignments of the isotropic resonances and the sideband patterns to atomic positions are also given in the figure.

that these two carbons possess identical isotropic chemical shifts. The two corresponding tensors reveal essentially identical δ_{22} values; however, they differ significantly in their δ_{11} and δ_{33} principal values by 12 and 10 ppm, respectively. These differences in the principal values are sufficient to clearly assign the observed chemical shifts to the two carbon atoms.

In solution, carbon atom C3′ in C possesses a higher shift than C2′ and the two carbons are separated by approximately 5 ppm. On the other hand, the EIM calculations predict a reversed order and an approximately doubled separation for these two carbon atoms.

EIM Calculations. The number of molecules per unit cell, Z, the number of atoms per unit cell, N_{uc}, the EIM parameter, N_i, and the Ewald parameters, N and N_T, used in the EIM calculations on A, Gdh, dT, and C are given in Table 8. In addition, the table shows the rms values for the correlations between the simulated potentials and the actual Ewald potentials. In all Ewald calculations, $N_1 = 200$ and $N_C = 500$ are utilized. A size of zone 1 given by $N_1 = 200$ was found to be sufficient to include the nucleoside molecules of interest, and the size of zones 1 and 2 together with $N_C = 500$ was shown to be adequate. Ewald calculations with point charge array sizes given by $N = 2$ were conducted and were found to require meaningless high partial charges in zone 3 of the arrays depending on the nucleoside under investigation. Furthermore, the rms values obtained in these calculations turned out to be unacceptable high in the order of tenths of volts or even volts. This clearly indicates that point charge arrays with $N = 2$ are too small to reasonably simulate the Ewald potentials in the nucleoside crystal studied here. Consequently, the results from EIM calculations with $N = 2$ are irrelevant and not further discussed. In agreement with previous findings,[21,36] the accuracy with which the Ewald potential is simulated generally increases with the size of the point charge array for constant sizes of zones 1 and 2. It was also observed previously[21,36] that a point charge array of approximately $N_T = 10\,000$ results in an rms value of approximately 1 μV. However, the data in Table 8 show that notably larger point charge arrays are required to reach the same accuracy in Ewald calculations on the nucleosides. Clear trends for the rms values obtained in the Ewald calculations on the nucleosides as functions of the parameters N, Z, and N_{uc} are not found, and the set of parameters that results in a certain rms value varies for each nucleoside under investigation.

Neutron Diffraction Data and Optimized Proton Positions. Table 9 shows the rms deviations of the bond distances, bond

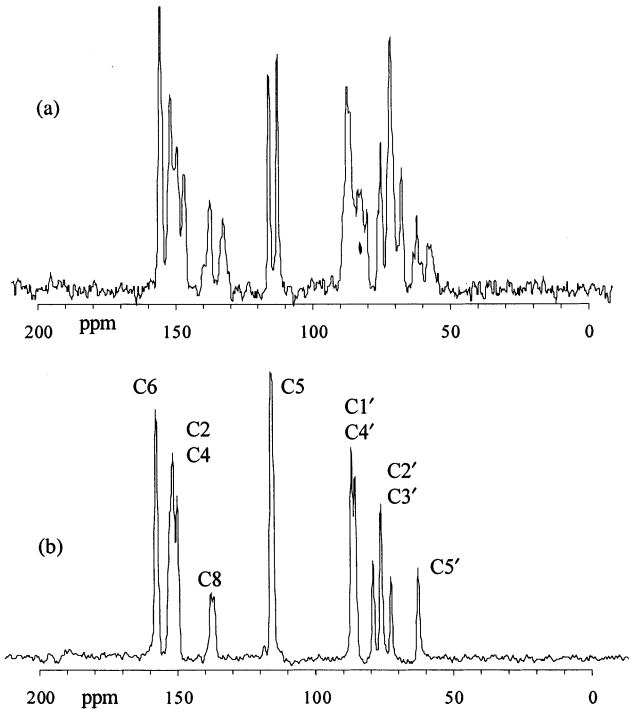

Figure 4. The ^{13}C TOSS CPMAS spectra of G in (a) a nonstoichiometric state of hydration and (b) the dihydrated state.

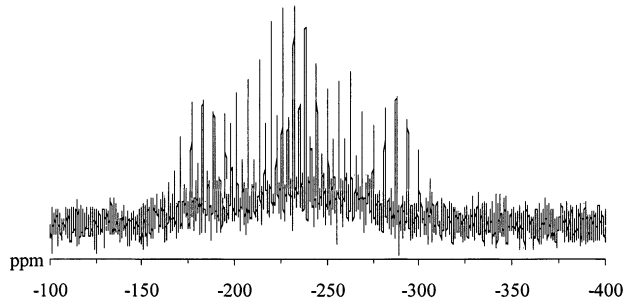

Figure 5. ^{15}N slow-spinning 1-D spectrum of dT.

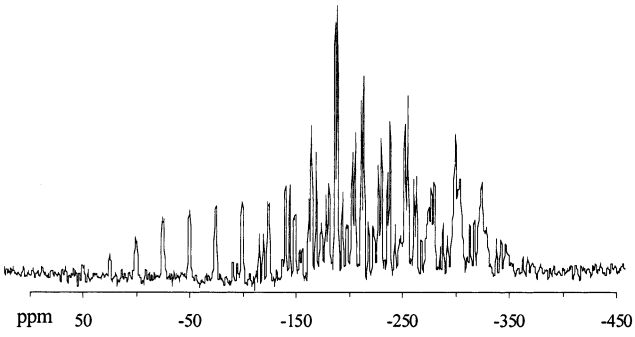

Figure 6. ^{15}N slow-spinning 1-D spectrum of Gdh.

angles, and dihedral angles obtained by X-ray[63] diffraction and in the ISO/H-OPT/4 and EIM/H-OPT/4 calculations on A from the corresponding accurate neutron diffraction values. The table distinguishes between distances and angles that involve hydrogen atoms bonded to carbon atoms and to oxygen or nitrogen atoms, due to their very different character. As expected, the C−H, N−H, and O−H X-ray distances reveal the largest rms deviations from the neutron diffraction distances of about 0.15 Å. All the X-ray distances appear to be significantly too short. The C−H distances are equally well reproduced in the ISO/H-OPT and the EIM/H-OPT/4 calculations with rms values around 0.005 Å. However, the N−H and O−H distances are reproduced with a detectable, slightly higher accuracy of close to 0.01 Å in the EIM/H-OPT/4 calculations. Essentially the same trends as observed for the accuracies with which the neutron diffraction bond distances are reproduced apply for the bond angles. The neutron diffraction bond angles are reproduced with a remarkable precision of 1.3° in the EIM/H-OPT/4 calculations. The data in Table 9 show that optimizing dihedral angles for O−H and N−H groups for isolated nucleoside molecules leads

(63) Lai, T. F.; Marsh, R. E. *Acta Crystallogr., Sect. B* **1972**, *28*, 1982−1989.

Table 4. Experimental ^{13}C and ^{15}N Chemical Shift Tensor Principal Values, the Corresponding Averages, and the Isotropic MAS and Solution Chemical Shift Values for A[a]

atom	δ_{11}	δ_{22}	δ_{33}	δ_{avg}[b]	δ_{MAS}	δ_{Soln}
C2	239	158	66	154.5	154.8	153.3
C4	221	166	58	148.3	148.5	149.9
C5	167	145	47	119.7	119.7	120.2
C6	222	191	52	155.2	155.2	157.0
C8	216	136	61	137.8	137.8	141.0
C1′	109	92	76	92.3	92.3	89.0
C2′	100	75	38	71.9	71.2	71.6
C3′	88	78	59	75.0	75.0	74.5
C4′	113	93	48	84.9	84.9	86.8
C5′	86	68	34	62.8	62.7	62.5
N1	−29	−84	−360	−157.6	−157.4	−144.3
N3	−27	−82	−386	−164.7	−164.5	−157.0
N7	40	−94	−379	−144.2	−144.1	−140.1
N9	−148	−198	−281	−209.0	−208.9	−209.3
NH_2	−229	−325	−334	−296.0	−296.5	−297.1

[a] Values are given in ppm. [b] $\delta_{avg} = (1/3)(\delta_{11} + \delta_{22} + \delta_{33})$.

Table 5. Experimental ^{13}C and ^{15}N Chemical Shift Tensor Principal Values, the Corresponding Averages, and the Isotropic MAS and Solution Chemical Shift Values for Gdh[a]

atom	δ_{11}	δ_{22}	δ_{33}	δ_{avg}[b]	δ_{MAS}	δ_{Soln}
C2	223	165	66	151.3	152.2	153.3
	223	165	66	151.3		
C4	223	165	66	151.3	151.4	149.9
	223	165	66	151.3	150.0	
C5	159	138	49	115.1	115.2	120.2
	160	140	49	116.0	115.9	
C6	237	154	82	157.7	157.7	157.7
	237	154	82	157.7	157.7	
C8[c]	214	141	59	138.2	138.2	141.0
	211	134	66	136.9	136.9	
C1′	112	89	54	85.2	85.2	89.0
	112	89	54	85.2	85.2	
C2′[c]	105	77	45	75.7	75.8	71.6
	103	79	55	78.9	78.9	
C3′[c]	89	75	53	72.3	72.3	74.5
	86	80	62	76.2	76.2	
C4′	108	92	60	86.6	86.6	86.8
	108	92	60	86.6	86.6	
C5′	84	65	39	62.7	62.7	62.5
	84	65	39	62.7	62.7	
N1[c]	−143	−235	−307	−227.4	−227.5	−233.3
	−149	231	−308	−230.2	−230.2	
N3[c]	−109	−164	−381	−218.2	−218.2	−214.8
	−100	−159	−384	−214.1		
N7	24	−104	−368	−149.1	−149.0	−132.7
	38	−99	−382	−147.8	147.7	
N9[d]	−150	−199	−291	−213.3	−213.4	−210.6
	−152	−189	−292	−211.2	211.2	
NH_2	−249	−328	−334	−303.5	−303.3	−307.2
	−241	−310	−348	−299.4	−299.4	

[a] Values are given in ppm. [b] $\delta_{avg} = (1/3)(\delta_{11} + \delta_{22} + \delta_{33})$. [c] Assignment of resonances to the two distinct molecules per asymmetric unit possible.

Table 6. Experimental ^{13}C and ^{15}N Chemical Shift Tensor Principal Values, the Corresponding Averages, and the Isotropic MAS and Solution Chemical Shift Values for dT[a]

atom	δ_{11}	δ_{22}	δ_{33}	δ_{avg}[b]	δ_{MAS}	δ_{Soln}
C2	226	124	96	148.6	148.6	151.5
C4	243	166	85	164.5	164.6	164.8
C5	187	117	24	109.4	109.7	110.4
C6	238	128	42	135.6	135.6	137.2
C1′	122	88	47	85.3	85.2	84.9
C2′	59	39	20	39.1	39.1	40.3
C3′	86	77	50	70.6	70.6	71.5
C4′	112	87	57	85.1	85.2	88.3
C5′	82	65	31	59.3	59.3	62.2
CH_3	17	10	1	9.3	9.1	13.2
N1	−160	−228	−306	−231.5	−231.5	−236
N3	−156	−230	−279	−222.4	−222.4	−224

[a] Values are given in ppm. [b] $\delta_{avg} = (1/3)(\delta_{11} + \delta_{22} + \delta_{33})$.

Table 7. Experimental ^{13}C and ^{15}N Chemical Shift Tensor Principal Values, the Corresponding Averages, and the Isotropic MAS and Solution Chemical Shift Values for C[a]

atom	δ_{11}	δ_{22}	δ_{33}	δ_{avg}[b]	δ_{MAS}	δ_{Soln}
C2	222.8	157.0	93.2	157.7	157.5	156.8
C4	248.2	204.2	49.0	167.2	167.3	166.6
C5	175.9	94.6	16.9	95.8	95.8	95.6
C6	240.7	151.5	34.8	142.4	142.3	142.7
C1′	111.8	90.0	76.0	92.6	92.7	90.1
C2′	89.2	78.2	59.4	75.9	75.6	70.4
C3′	96.9	72.4	30.3	66.5	66.5	75
C4′	113.8	93.3	44.4	84.1	84.0	85.2
C5′	85.1	65.4	29.8	60.1	60.1	61.8
N1	−143	−218	−311	−224.0	−223.9	−229.9
N3	−82	−138	−325	−181.6	−181.5	−172.3
NH_2	−215	−310	−334	−286.3	−286.3	−289.0

[a] Values are given in ppm. [b] $\delta_{avg} = (1/3)(\delta_{11} + \delta_{22} + \delta_{33})$.

Table 8. Selected Crystallographic Information and Ewald Parameters for A, Gdh, dT, and C[a]

				$N = 3$		$N = 4$	
nucleoside	Z	N_{uc}	N_i	N_T	rms	N_T	rms
A	2	64	4	13 824	18	32 762	0.93
Gdh	4	156	4			79 872	0.59
dT	4	124	4	26 784	290	63 488	1.7
C	4	120	5	25 920	68	61 440	1.9

[a] The rms values are given in μV.

Table 9. Comparison of the X-ray Proton Positions and the Optimized Proton Positions Obtained in the Iteration Procedure of the EIM/H-OPT/4 Calculation and in ISO/H-OPT Calculations to the Neutron Diffraction Proton Positions of Adenosine[a]

	bond lengths		bond angles		dihedral angles	
method	O–H/N–H	C–H	O–H/N–H	C–H	O–H/N–H	C–H
EIM/H-OPT/4	0.0095	0.0055	1.3	0.8	4.7	1.1
ISO/H-OPT	0.0202	0.0052	3.4	0.9	17.3	1.1
X-ray	0.1359	0.1565	4.4	1.4	4.8	5.6

[a] The table shows rms deviations of bond distances, bond angles, and dihedral angles from the corresponding experimental neutron diffraction values. The rms values for bond lengths are given in Å, and for bond angles and dihedral angles in deg.

to series errors in these angles due to the neglect of intermolecular interactions.

The optimizations of proton positions for Gdh,[60] dT,[64] and C[65] from their X-ray positions in the EIM/H-OPT/4 calculations primarily result in significant changes of the bond distances, which appear to be significantly too short in all cases. Bond angles and dihedral angles in the X-ray and optimized geometries involving hydrogen atoms are generally comparable and differ noticeable only in a few cases.

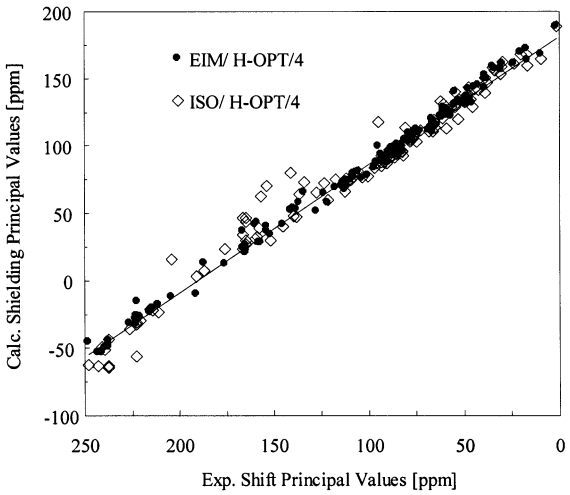

Figure 7. Plot of the ^{13}C calculated shielding tensor principal values versus the experimental chemical shift tensor principal values for A, Gdh, dT, and C, obtained in EIM/H-OPT/4 and ISO/H-OPT/4 calculations.

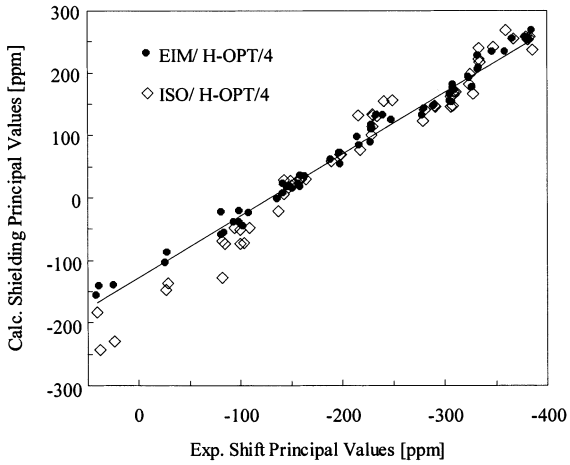

Figure 8. Plot of the ^{15}N calculated shielding tensor principal values versus the experimental chemical shift tensor principal values for A, Gdh, dT, and C, obtained in EIM/H-OPT/4 and ISO/H-OPT/4 calculations.

Calculated Principal Values. The calculated ^{13}C and ^{15}N shielding tensor principal values obtained in ISO/X-RAY, ISO/H-OPT, ISO/H-OPT/4, and EIM/H-OPT/4 calculations on all four nucleosides are correlated with the corresponding experimental chemical shift tensor principal values. Figures 7 and 8 show the ^{13}C and ^{15}N shielding-shift correlation plots, respectively, obtained in ISO/H-OPT/4 and EIM/H-OPT/4 calculations. The theoretical slopes and intercepts for ^{13}C and ^{15}N shielding-shift correlations are −1 for both nuclei and the chemical shift value for the bare nuclei of 188.1[66] and −135.0 ppm,[67,68] respectively. The slopes and intercepts, with the respective uncertainties, and the rms values obtained in linear fits for the four theoretical approaches listed above in this study are given

(64) Young, D. W.; Tollin, P.; Wilson, H. R. *Acta Crystallogr., Sect. B* **1969**, *25*, 1423−1432.
(65) Lirong, C.; Craven, B. M. *Acta Crystallogr., Sect. B* **1995**, *51*, 1081−1097.
(66) Jameson, A. K.; Jameson, C. J. *Chem. Phys. Lett.* **1987**, *134*, 461−466.
(67) Jameson, C. J.; Jameson, A. K.; Burrell, P. M. *J. Chem. Phys.* **1980**, *73*, 6013−6020.
(68) Jameson, C. J.; Jameson, A. K.; Oppusunggu, D.; Wille, S.; Burrell, P. M. *J. Chem. Phys.* **1981**, *74*, 81−88.

Table 10. Fitting Data for ^{13}C and ^{15}N Shielding-Shift Correlations Obtained in Various Shielding Tensor Calculations on All Four Nucleosides[a]

	slope	intercept	rms
	^{13}C		
ISO/X-RAY	−1.02(±0.01)	194(±2)	10.1
ISO/H-OPT	−0.94(±0.01)	181(±1)	9.2
ISO/H-OPT/4	−0.94(±0.01)	181(±2)	9.4
EIM/H-OPT/4	−0.95(±0.01)	181(±1)	4.9
	^{15}N		
ISO/X-RAY	−1.19(±0.03)	−172(±8)	28.5
ISO/H-OPT	−1.13(±0.03)	−164(±7)	24.3
ISO/H-OPT/4	−1.12(±0.03)	−163(±7)	23.9
EIM/H-OPT/4	−0.99(±0.01)	−128(±3)	12.6

[a] Slopes are dimensionless; intercepts and rms values are given in ppm.

in Table 10. All four theoretical approaches reveal similar and reasonable slopes and intercepts. The ISO/X-RAY calculations predict the experimental ^{13}C principal values with the highest uncertainty of 10.1 ppm. The rms value of the correlation is scarcely reduced to 9.2 and 9.4 ppm for the ISO/H-OPT and ISO/H-OPT/4 calculations, respectively, when optimized proton positions are utilized in the calculations. It appears that the slightly more accurate proton positions generated in the ISO/H-OPT/4 calculations do not result in a detectable lower rms value compared to the ISO/H-OPT calculations, as both approaches predict the experimental principal values with essentially the same accuracy. A significant reduction of the rms value to 4.9 ppm is observed when electrostatic crystal potentials are included in the shielding calculations to simulate the intermolecular interactions by applying the EIM. This rms value for the ^{13}C shielding-shift correlation corresponds to a relative error of about 2% for a chemical shift range of 250 ppm and approaches experimental errors. The data in Table 10 reveal that the differences between the rms values obtained for the ^{15}N shielding-shift correlations in ISO/X-RAY, ISO/H-OPT, ISO/H-OPT/4, and EIM/H-OPT calculations are notably more pronounced and the range of rms values observed is larger than for the ^{13}C correlations. ISO/X-RAY calculations produce a poor ^{15}N shielding-shift correlation with an rms value of 28.5 ppm and a slope and intercept that deviate significantly from the corresponding theoretical values. The rms value, slope, and intercept of the correlation are reduced notably when the proton positions are optimized in the ISO/H-OPT calculations; nevertheless, the rms value remains intolerably high at 24.3 ppm. Utilizing the slightly more accurate proton positions in ISO/H-OPT/4 calculations only insignificantly lowers the rms value of the correlation to 23.9 ppm. However, as for the ^{13}C shielding-shift correlations, the rms value for the^{15}N shielding-shift correlations is substantially reduced by about 50% to 12.6 ppm in the EIM/H-OPT/4 calculations that also yield an accurate slope and intercept. This rms value corresponds to a relative error of approximately 2.5% for a ^{15}N chemical shift range of more or less 500 ppm.

A comparison of the shielding-shift correlations obtained in the ISO/H-OPT/4 and EIM/H-OPT/4 calculations can be utilized to estimate the contribution to chemical shielding in the nucleosides arising from intermolecular interactions. Both calculations utilize the same, fairly accurate proton positions. Hence, differences in the calculated principal values obtained in these two approaches may predominantly be attributed to intermolecular interactions. EIM/H-OPT/4 and ISO/H-OPT/4

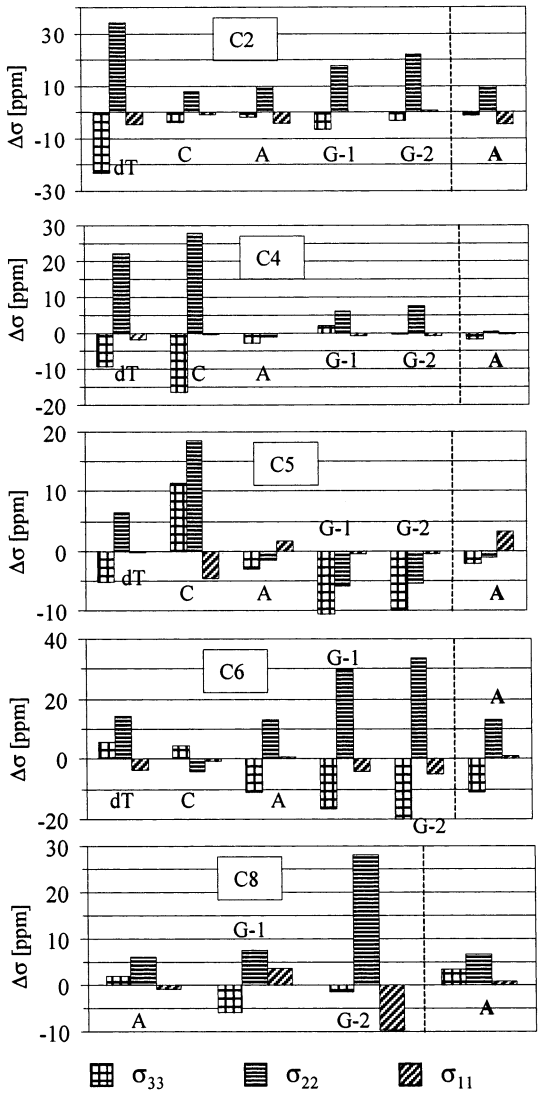

Figure 9. Contributions to the ^{13}C chemical shielding tensor components arising from electrostatic crystal potentials in the nucleic acid base carbons in A, G-1 G-2, dT, and C.

calculations essentially predict the principal values for the sugar carbons with the same accuracy of about 5 ppm. Exceptions are the σ_{22} and σ_{11} components for the C3′ atoms in Gdh, which differ by about 10 ppm between EIM/H-OPT/4 and ISO/H-OPT/4 calculations. Figure 9 illustrates the impact that crystal potentials have on the ^{13}C shielding tensors for the base carbon atoms. The differences between the individual ^{13}C shielding principal values obtained in ISO/H-OPT/4 and EIM/H-OPT/4 calculations, $\Delta\sigma_{H-OPT}$, are depicted by the bar graphs shown in Figure 9, separated for the five different types of carbons in the bases. Furthermore, Figure 9 displays data for the two different G molecules per asymmetric unit, denoted as G-1 and G-2. Due to the opposite directions of the shielding and the shift scale, the lowest shielding tensor principal value, σ_{33}, corresponds to the largest chemical shift tensor principal value, δ_{11}. Accordingly, σ_{22} and σ_{11} correspond to δ_{22} and δ_{33}, respectively, and $\sigma_{33} \leq \sigma_{22} \leq \sigma_{11}$. A negative $\Delta\sigma_{H-OPT}$ value for a given carbon atom corresponds to an increase in that shielding tensor component due to the inclusion of electrostatic crystal potentials in the calculations. Several principal values are corrected in the EIM/H-OPT/4 calculations by over 20 ppm,

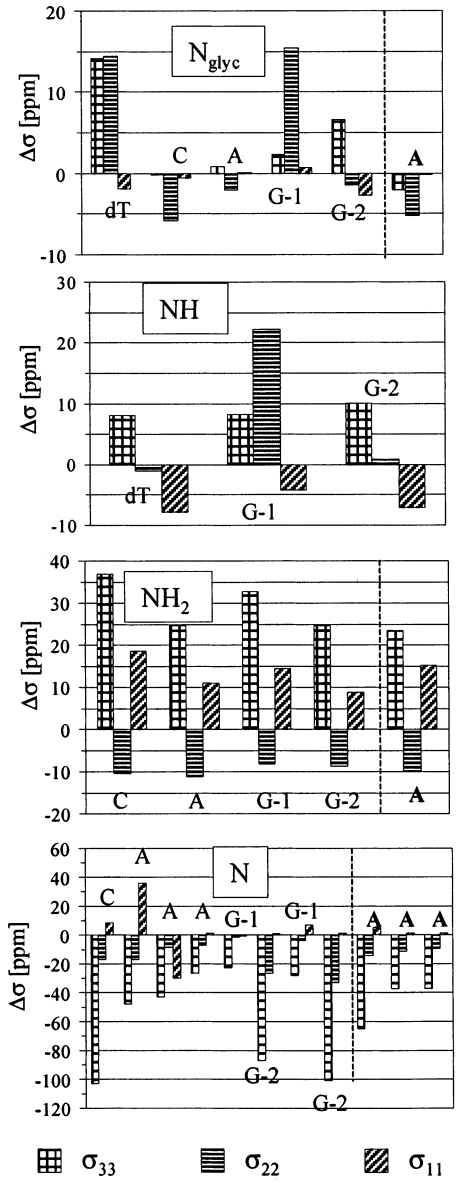

Figure 10. Contributions to the ^{15}N chemical shielding tensor components arising from electrostatic crystal potentials for the nitrogens in A, G-1, G-2, dT, and C.

and a few corrections even exceed 30 ppm. These outliers are almost exclusively found among the σ_{33} and σ_{22} in-plane chemical shielding tensor components of the base carbon atoms. However, overall, clear trends of individual ^{13}C tensor components due to the inclusion of electrostatic crystal potentials in the EIM/H-OPT/4 calculations are not observed. The $\Delta\sigma_{H-OPT}$ values for ^{15}N are depicted in the bar charts shown in Figure 10, separated for the four different types of nitrogens in nucleosides. The nitrogens that connect the bases to the sugar rings, nonprotonated nitrogens, protonated nitrogens, and NH_2 nitrogens are denoted as N_{glyc}, N, NH, and NH_2, respectively. As in Figure 9, Figure 10 contains data for the two different G molecules per asymmetric unit. Figure 10 reveals that the contributions to chemical shielding for ^{15}N nuclei arising from electrostatic crystal potentials are significantly more pronounced than for ^{13}C nuclei. Significant corrections of 10 ppm or above are observed for 50%, and tremendous corrections of 30 ppm or above are observed for 17% of the principal values. Two

Table 11. Fitting Data for ^{13}C and ^{15}N Shielding-Shift Correlations Obtained in Various Shielding Tensor Calculations on Selective Nucleosides[a]

	nucleosides	slope	intercept	rms
		^{13}C		
EIM-1/H-OPT/3	A, dT, C	−0.96(±0.01)	184(±1)	6.2
EIM/H-OPT/3	A, dT, C	−0.96(±0.01)	182(±1)	5.2
EIM-1/H-OPT/4	A, dT, C	−0.96(±0.01)	182(±1)	5.0
EIM/H-OPT/4	A, dT, C	−0.96(±0.01)	181(±2)	5.2
ISO/NEU	A	−0.94(±0.02)	180(±2)	5.1
EIM/NEU/4	A	−0.94(±0.02)	180(±2)	5.3
		^{15}N		
EIM-1/H-OPT/3	A, dT, C	−1.05(±0.03)	−144(±6)	16.4
EIM/H-OPT/3	A, dT, C	−0.99(±0.02)	−129(±4)	10.5
EIM-1/H-OPT/4	A, dT, C	−1.01(±0.02)	−135(±4)	11.4
EIM/H-OPT/4	A, dT, C	−0.99(±0.02)	−129(±4)	10.5
ISO/NEU	A	−1.12(±0.03)	−161(±8)	15.3
EIM/NEU/4	A	−1.02(±0.01)	−133(±3)	7.9

[a] Slopes are dimensionless; intercepts and rms values are given in ppm.

extreme cases are the enormous differences of over 100 ppm between the principal values obtained in ISO/H-OPT/4 and EIM/H-OPT/4 calculations. The smallest effects of including electrostatic crystal potentials in the calculations on the principal values are observed for N_{glyc} and NH nitrogens. The effects increase successively for NH_2 and N nitrogens, respectively. The $\Delta\sigma_{H-OPT}$ values for the N_{glyc} nitrogens show no clear trends. The principal shielding components for the N_{glyc} nitrogens in A and C seem not to be affected significantly by intermolecular interactions, whereas certain components of the N_{glyc} shielding tensors in dT and Gdh reveal a notable sensitivity to intermolecular interactions. All $\Delta\sigma_{H-OPT}$ values for the σ_{33} and σ_{11} tensor components for the NH nitrogens are found to be positive and negative, respectively, whereas $\Delta\sigma_{H-OPT}$ values for σ_{22} assume positive and negative values. σ_{22} for the NH atom in G-1 exhibits a significantly higher sensitivity to intermolecular interactions than the remaining NH nitrogen tensor components. A distinct trend is observed for the NH_2 nitrogens. Upon inclusion of electrostatic crystal potentials, σ_{33} and σ_{11} decrease, whereas σ_{22} increases. The magnitudes of the corresponding $\Delta\sigma_{H-OPT}$ values for C, A, G-1, and G-2 are also comparable. Remarkably large effects of including intermolecular interactions are found for the N nitrogens. For these nitrogens, the $\Delta\sigma_{H-OPT}$ values for σ_{33} and σ_{22} are negative, whereas positive and negative $\Delta\sigma_{H-OPT}$ values are observed for σ_{11}.

The contribution to chemical shielding arising from intermolecular interactions can be determined more accurately for A than for the remaining nucleosides by comparing the principal values obtained in the ISO/NEU and EIM/NEU/4 calculations performed on A. The neutron diffraction geometry for A contains accurate proton positions, and the EIM/NEU/4 calculations predict the ^{13}C and ^{15}N principal values for A remarkably well within 5 and 8 ppm, respectively, as shown in Table 11. Therefore, the differences between principal values for A obtained in ISO/NEU and EIM/NEU/4 calculations, $\Delta\sigma_{NEU}$, can be attributed exclusively to intermolecular interactions that are dominated by hydrogen bonding. The columns corresponding to the $\Delta\sigma_{NEU}$ values for the ^{13}C and ^{15}N shielding components in A are shown in Figures 9 and 10, respectively, to the right of the dotted lines in each bar chart, and are labeled with boldface letters. The data in these two figures reveal that the trends in the $\Delta\sigma_{NEU}$ values observed for A qualitatively agree with those found for the $\Delta\sigma_{H-OPT}$ values for all four nucleosides.

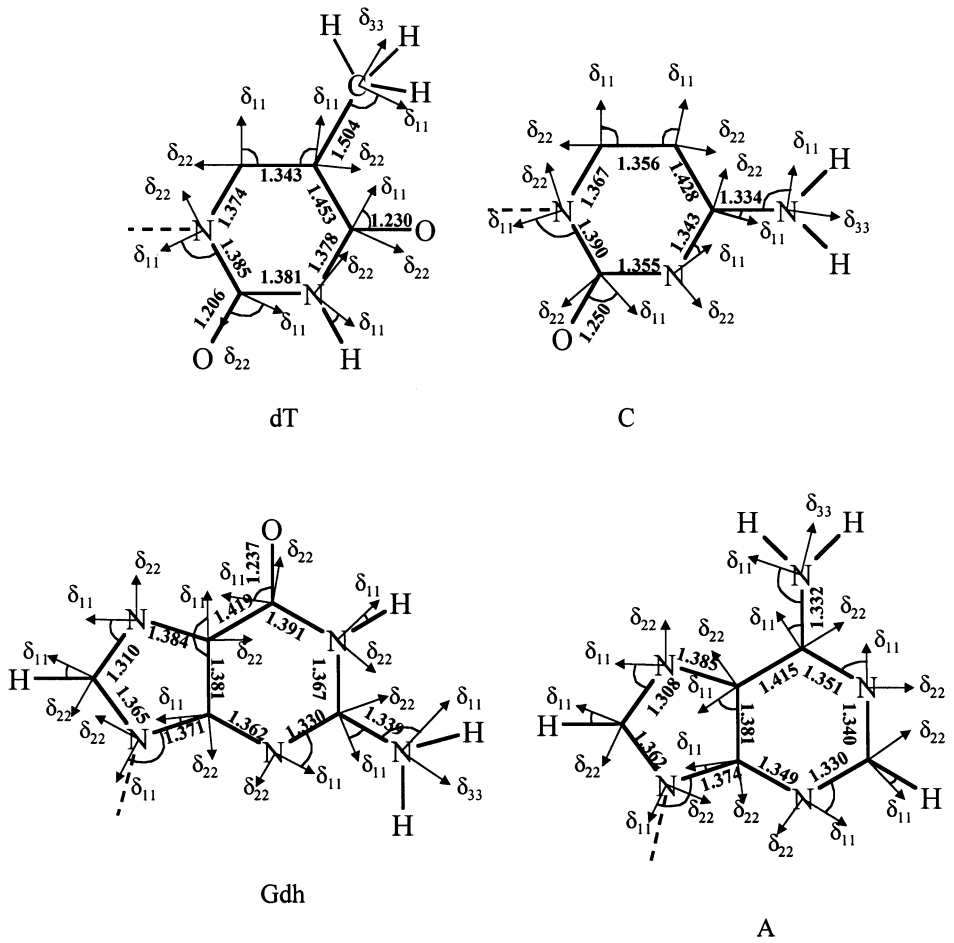

Figure 11. ^{13}C and ^{15}N chemical shift tensor orientations for the base carbon and nitrogen atoms and X-ray C−C, C−O, and C−N bond lengths (boldface numbers).

The fitting data for ^{13}C and ^{15}N shielding-shift correlations obtained in EIM-1/H-OPT/3, EIM/H-OPT/3, EIM-1/H-OPT/4, and EIM/H-OPT/4 calculations on A, dT, and C are given in Table 11. Overall, it appears to be advantageous in the calculation of ^{13}C principal values to complete the iteration procedure in the EIM until self-consistency of the point charge array is reached. However, this effect is barely detectable. When self-consistent point charge arrays are utilized, arrays with $N = 3$ and $N = 4$ reproduce the experimental ^{13}C principal values with equal accuracy. The experimental ^{15}N principal values are reproduced with a notably higher accuracy when self-consistent point charge arrays are utilized. As for the ^{13}C principal values, self-consistent point charge arrays with $N = 3$ and with $N = 4$ reproduce the experimental ^{15}N principal values with essentially identical accuracy.

Chemical Shift Tensor Orientations. The ISO/H-OPT/4 and EIM/H-OPT/4 calculations assign the general orientations of the chemical shift tensor components for the base carbon and nitrogen atoms in agreement. Figure 11 depicts the general orientations of the two in-plane chemical shift tensor components for the base carbon and nitrogen atoms. For these carbons and nitrogens, the δ_{11} and δ_{22} components lay within the planes of the bases, and consequently, δ_{33} is oriented perpendicular to this plane. The CH_3 and NH_2 groups possess δ_{11} and δ_{33} as the in-plane components and δ_{22} as the perpendicular tensor component. The exact angles that the ^{13}C and ^{15}N tensors assume with respect to the molecular frames of the nucleosides differ between the ISO/H-OPT/4 and EIM/H-OPT/4 calculations for several carbon and nitrogen atoms. Table 12 gives the angles in degrees that the ^{13}C and ^{15}N δ_{11} shift tensor components assume with the selected bonds in Figure 11. These data reveal that the angles for δ_{11} orientations obtained in shielding calculations on isolated nucleoside molecules are corrected significantly in the EIM

Table 12. Angles That the ^{13}C and ^{15}N Chemical Shift Tensor δ_{11} Components for the Base Carbons and Nitrogens Assume with the Bonds Depicted in Figure 11[a]

nucleoside	method	C2	C4	C5	C6	C8	CH_3
A	ISO/H-OPT/4	3	0	43	1	27	
	EIM/H-OPT/4	3	3	44	1	27	
Gdh	ISO/H-OPT/4	**30**	9	**151**	80	27	
	EIM/H-OPT/4	**43**	3	**181**	78	28	
dT	ISO/H-OPT/4	91	79	105	95		86
	EIM/H-OPT/4	92	71	106	90		85
C	ISO/H-OPT/4	**80**	6	111	94		
	EIM/H-OPT/4	**69**	7	109	91		

nucleoside	method	N1	N3	N7	N9	NH_2
A	ISO/H-OPT/4	**48**	**47**	50	130	98
	EIM/H-OPT/4	**65**	**61**	54	130	98
Gdh	ISO/H-OPT/4	12	58	**48**	143	97
	EIM/H-OPT/4	16	53	**58**	142	95
dT	ISO/H-OPT/4	86	8			
	EIM/H-OPT/4	86	9			
C	ISO/H-OPT/4	105	**42**			96
	EIM/H-OPT/4	100	**28**			95

[a] Values are given in deg.

calculations by 10° or more in seven cases. The corresponding angles are given in boldface numbers. However, these reorientations of the shielding tensors due to electrostatic crystal potentials do not follow clear trends and do not reflect the general strong sensitivity of the nitrogen shielding tensor principal values to electrostatic crystal effects.

The X-ray C−C, C−O, and C−H bond lengths for A, Gdh, dT, and C are also given in Figure 11 next to the respective bonds in angstroms (boldface numbers). These values illustrate that the orientations of the ^{13}C tensor components obtained in EIM/H-OPT/4 calculations as indicated in Figure 11 follow the rules established for trigonal sp^2 carbon atoms in polycyclic aromatic hydrocarbons (PAHs)[69] and in carbonates and thiocarbonates.[15] If two adjacent, more or less equal bonds have smaller π-characters than the third adjacent bond, δ_{11} tends to be oriented approximately perpendicular to the adjacent bond with the highest π-character. This is observed for the carbonyl carbon atoms, C2 and C4, C2, and C6, in dT, C, and Gdh, respectively. A comparison with a typical C−O double-bond length of 1.23 Å in aldehydes[70] clearly reveals the double-bond character for these bonds. Furthermore, the larger π-character of the C6−C5 bonds in dT and C suggested by the approximately perpendicular δ_{11} orientation to these bonds is supported by the corresponding bond distances. The C6−C5 bonds in dT and C are significantly shorter, 1.343 and 1.356 Å, respectively, than typical partial C−C double bonds and are closer to lengths of typical C−C single bonds.[70] When two bond orders of adjacent π-bonds are similar and larger than that for the third adjacent bond, δ_{11} lies approximately along the third bond with the lower bond order. This situation applies to the C8 and C2 carbon atoms in A and Gdh and to C5 in A (see bond lengths in Figure 11). However, the ^{13}C shift tensor orientations and principal values for the bridgehead carbons, C5 in Gdh and C4 in A and Gdh, exhibit deviations from the established rules. C5 in Gdh reveals a different orientation than the equivalent carbon in A, which could be attributed to the nearly axial symmetry for the C5 tensor in Gdh. However, the orientation that is observed for C5 in Gdh does not correlate with the adjacent bond lengths. The comparable three adjacent bonds about the C4 carbons in A and Gdh are expected to result in a nearly axially symmetric tensor with δ_{11} close to δ_{22}. Nonetheless, the data in Tables 4 and 5 reveal that both tensors deviate considerably from axial symmetry and are closer to being centro symmetric. Overall, the deviations of certain ^{13}C tensor orientations and principal values from the expected values can likely be attributed to the different character of C−N bonds as compared to C−C bonds.

The chemical shift tensor orientations determined for the base nitrogens in EIM/H-OPT/4 calculations as indicated in Figure 11 are in agreement with the orientations previously established for nitrogen-containing heterocycles.[3] δ_{11} or δ_{22} are the two in-plane components. Depending on the type of nitrogen, either δ_{11} or δ_{22} assumes an approximately tangential orientation with respect to the aromatic ring, and consequently the remaining component is found in an approximately radial orientation. Figure 12 depicts the magnitudes of the ^{15}N chemical shift tensor principal values as functions of their orientations for the four different types of nitrogens present in the nucleosides. The

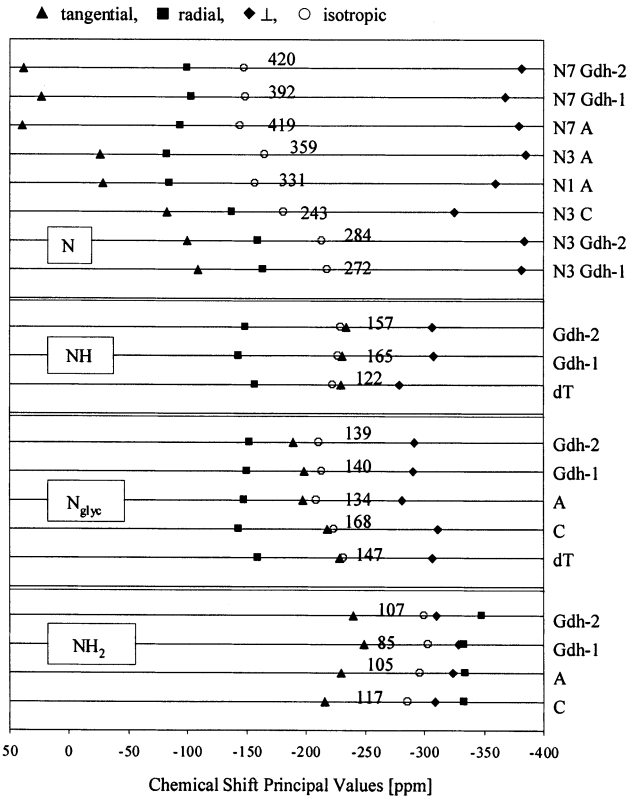

Figure 12. Magnitudes of the ^{15}N chemical shift tensor principal values as functions of their orientations for the four different types of nitrogens present in the nucleosides (solid symbols). The figure also displays the trends of the corresponding isotropic MAS shift values (open circles) and the tensor spans in ppm (numbers).

corresponding isotropic MAS values and the tensor spans in ppm are also given in Figure 12. The N nitrogens possess δ_{11} and δ_{22} as the tangential and radial components, respectively. This order is reversed for the NH and the N_{glyc} nitrogens. For all ring nitrogens, the perpendicular component has the lowest chemical shift. The chemical shift tensor orientations shown in Figure 12 arise from the fact that the largest shielding component, δ_{11}, is generally oriented perpendicular to the plane defined by the highest occupied molecular orbital (HOMO)−lowest unoccupied molecular orbital (LUMO) pair with the smallest energy gap.[71,72] The tangential component for N nitrogens is dominated by the n−π* transition with a relatively small energy gap, making the tangential component the largest shift component for these nitrogens. On the other hand, the σ−π* transitions involving a considerably larger energy gap dominate the tangential direction for the substituted nitrogens, NH and N_{glyc}. This causes the tangential components to become considerably smaller in these nitrogens and to switch orientation with the radial component. Since the radial and the $\delta_{\perp}$ components for all three types of aromatic nitrogens, N, NH, and N_{glyc}, are always dominated by σ−π* transitions, these two components do not vary over such a wide chemical shift range as the tangential component does.

Figure 12 reveals that the N nitrogen tensors exhibit the largest chemical shift anisotropies, whereas NH and N_{glyc} reveal similar, considerably narrower tensor spans. Remarkably large

(69) Facelli, J. C.; Grant, D. M. *Top. Stereochem.* **1989**, *19*, 1−62.
(70) *CRC Handbook of Chemistry and Physics*, 63rd ed.; Weast, R. C., Ed.; CRC Press: Boca Raton, FL, 1983.
(71) Facelli, J. C.; Grant, D. M.; Michl, J. *Int. J. Quantum Chem.* **1987**, *31*, 45−55.
(72) Solum, M. S.; Facelli, J. C.; Grant, D. M.; Michl, J. *J. Am. Chem. Soc.* **1986**, *108*, 6464−6470.

tensor spans of about 400 ppm are observed for the N7 nitrogens in A and Gdh. The ^{15}N tensor principal values and tensor spans measured for the nucleosides in this work are comparable with those recorded by Hu et al. for the corresponding purine and pyrimidine bases, adenine, guanine, thymine, and cytosine.[6] These authors reported three major trends for the ^{15}N shift tensor principal values and orientations: (1) the largest effects of including intermolecular interactions are observed for the two in-plane components; (2) for N nitrogens, including intermolecular interactions increases the in-plane shielding; and (3) for NH and NH_2 nitrogens, trend 2 is reversed. For obvious reasons, the tensors for the N_{glyc} nitrogens in the nucleosides differ significantly from the corresponding NH protons in the individual bases. However, Figure 10 reveals that the trends observed for the remaining nitrogens in the nucleosides are in agreement with the trends obtained by Hu et al. The largest effects are observed for the in-plane shielding tensor components for the nucleosides. Moreover, upon the inclusion of electrostatic crystal potentials, the in-plane shielding components for N nitrogens increase, and those for NH and NH_2 nitrogens decrease.

The NH_2 chemical shift tensor orientations differ from those just discussed for the aromatic nitrogens. The NH_2 nitrogens lie within the planes of the aromatic rings; however, the protons are located above and below these planes. For the NH_2 groups, δ_{11} and δ_{33} assume approximately a perpendicular and an aligned orientation, respectively, with respect to the $C_{ring}-NH_2$ bond. In the CH_3 group in C, δ_{11} and δ_{33} assume approximately a perpendicular and an aligned orientation, respectively, with respect to the $C_{ring}-CH_3$ bond. These orientations are observed for the methyl groups in the carbonate and thiocarbonate anions[15] and previously in several organic molecules.[72]

Conclusions

EIM calculations significantly improve the precision with which the experimental ^{13}C and ^{15}N chemical shielding tensor principal values for adenosine, guanosine dihydrate, 2′-deoxythymidine, and cytidine are reproduced over calculations on the corresponding isolated molecules with proton-optimized geometries. ^{13}C and ^{15}N chemical shift tensors are computed in EIM calculations within approximately 5 and 12 ppm, respectively, which corresponds to a relative error on the respective chemical shift scales of about 2% and 2.5%, respectively. ^{13}C and ^{15}N shielding calculations based upon X-ray proton positions yield principal values that correlate significantly less well with the corresponding experimental values. The error margin and the improvement due to the EIM are considerably more pronounced for ^{15}N shielding calculations.

The EIM appears to be adequate to simulate the effects of the strong 3-D hydrogen-bonding network in the nucleoside crystals on chemical shielding. The differences between principal values obtained in EIM calculations and in calculations on isolated molecules with proton positions optimized iteratively inside a point charge array are used to estimate the contributions to chemical shielding arising from intermolecular interactions. The ^{13}C and ^{15}N chemical shift tensor orientations are reliably assigned in the molecular frames of the nucleosides based upon the results obtained in EIM calculations. Moreover, the ^{13}C and ^{15}N chemical shift tensor orientations and principal values correlate for the nucleosides with molecular structure and crystallographic environment, and these trends agree with data obtained previously for related compounds.

It is shown that the accuracy of the EIM may be used to assign observed solid-state ^{13}C and ^{15}N resonances to atomic positions, which is especially helpful in cases in which peak positions moved between the solution and solid state. Utilization of the EIM in conjunction with the FIREMAT data analysis approach proved to be very efficient to overcome assignment problems due to severe spectral overlap and to extract the corresponding principal values. The neutron diffraction data on adenosine are used to demonstrate that the iteration procedure of the EIM may be utilized effectively to generate OH and NH proton positions that are considerably closer to the corresponding neutron diffraction data, as compared to positions obtained from calculations on the isolated nucleoside molecules.

Shielding tensor calculations with systematic variations of certain Ewald parameters reveal that overall, more accurate results are produced when self-consistent point charge arrays are utilized. This effect is significant for ^{15}N shielding tensors and barely detectable for ^{13}C shielding tensors. It is further found that the precision of shielding tensor calculations is invariant to the size of the point charge array generated, given that a certain minimum size is exceeded.

Acknowledgment. This work was supported by the U.S. Department of Energy under DOE No. DE-FG03-94ER14452 and by the National Institutes of Health under GM 08521-40. Computer time for this study was provided by an allocation from the University of Utah Center of High Performance Computing.

JA012485C